INTERNATIONAL JOURNAL FOR NUMERICAL METHODS IN FLUIDS
Int. J. Numer. Meth. Fluids 2011; **00**:1–27
Published online in Wiley InterScience (www.interscience.wiley.com). DOI: 10.1002/fld

An efficient and stable finite element solver of higher order in space and time for nonstationary incompressible flow

S. Hussain[1]*, F. Schieweck[2], S. Turek[1]

[1] *Institut für Angewandte Mathematik (LS III), TU Dortmund, Germany*
[2] *Institut für Analysis und Numerik, Otto-von-Guericke-Universität Magdeburg, Germany*

SUMMARY

In this paper, we extend our work for the heat equation [1] and for the Stokes equations [2] to the nonstationary Navier-Stokes equations. We present fully implicit *continuous* Galerkin-Petrov (cGP) and *discontinuous* Galerkin (dG) time stepping schemes for incompressible flow problems which are, in contrast to standard approaches like for instance the Crank-Nicolson scheme, of higher order in time. In particular, we implement and analyze numerically the higher order dG(1) and cGP(2)-methods which are super-convergent of 3rd, resp., 4th order in time, while for the space discretization, the well-known LBB-stable finite element pair Q_2/P_1^{disc} is used. The discretized systems of nonlinear equations are treated by using the Newton method, and the associated linear subproblems are solved by means of a monolithic multigrid method with a blockwise Vanka-like smoother [3]. We perform nonstationary simulations for two benchmarking configurations to analyze the temporal accuracy and efficiency of the presented time discretization schemes. As a first test problem, we consider a classical *flow around cylinder* benchmark [4]. Here, we concentrate on the nonstationary behavior of the flow patterns with periodic oscillations and examine the ability of the different time discretization schemes to capture the dynamics of the flow. As a second test case, we consider the nonstationary *flow through a Venturi pipe* [5, 6]. The objective of this simulation is to control the instantaneous and mean flux through this device. Copyright © 2011 John Wiley & Sons, Ltd.

Received ...

KEY WORDS: Discontinuous Galerkin method, continuous Galerkin-Petrov method, incompressible Navier-Stokes equations, monolithic Newton-multigrid method, Vanka smoother, CFD benchmarking

*Correspondence to: Institut für Angewandte Mathematik (LS III), TU Dortmund, Vogelpothsweg 87, 44227 Dortmund, Germany. E-mail: shafqat.hussain@math.tu-dortmund.de

Contract/grant sponsor: The authors want to express their gratitude to the German Research Association (DFG) and the Higher Education Commission (HEC) of Pakistan for their financial support of the study; contract/grant number: SCHI 576/2-1, TU 102/35-1 and LC06052 by MSMT

1. INTRODUCTION

For solving nonstationary flow problems, it is very common to discretize partial differential equations (PDEs) first in space and then in time, known as the 'Method of Lines'. This approach creates a system of ordinary differential equations (ODEs) which might be solved by state-of-the-art ODE integrators. However, the grid points of the spatial mesh have to stay fixed in time or are often subject to certain constraints, as for example in the case of moving mesh methods, so that these methods often have difficulties in changing the spatial mesh from time step to time step. On the other hand, the Rothe method, which performs first the semi-discretization in time, allows a fully adaptive integration of time dependent PDEs. A class of time discretization schemes which is based on Rothe's method is the *continuous* Galerkin-Petrov discretization (cGP(k)-methods) and the *discontinuous* Galerkin (dG(k)) approach. The cGP-method has already been used by Aziz and Monk [7] (but not under this name) for the linear heat equation in which case they could prove optimal error estimates as well as superconvergence results at the discrete time points τ_n. Currently, extensive tests regarding the higher order accuracy in time have been performed for the heat equation in [1] and for the Stokes equations in [2].

In this paper, we extend these numerical studies to the nonstationary Navier-Stokes equations. In particular, we implement and analyze numerically the (fully implicit) cGP(2)-method which is found, at comparable numerical cost per time step, to be of higher order than classical schemes like Crank-Nicolson or BDF methods, namely of order 3 in the whole time interval and superconvergent of order 4 in the discrete time points. Since we obtain such superconvergence results at t_n for the velocity only, it is also desirable to get a higher order pressure at the same time points, for instance for the computation of the hydrodynamic forces in CFD problems such as drag, lift etc. Therefore, we perform additionally a special postprocessing based on a simple local interpolation procedure as described in [2]. Moreover, the corresponding spatial discretization is carried out by using biquadratic finite elements (Q_2) for the velocity and discontinuous linear elements (P_1^{disc}) for the pressure which are of similar high order accuracy in space, namely of third order for the velocity and second order for the pressure measured in the L^2-norm. On each time interval, the cGP(2)-method as well as the dG(1)-method lead to a 2×2 nonlinear block-system of Navier-Stokes equations in space. The resulting discretized systems of nonlinear equations, which are characterized as coupled saddle point problems, are treated by means of the Newton method, and the associated linear subproblems are solved using a monolithic multigrid solver with a local pressure Schur complement type smoother of Vanka type [3].

For a systematic comparison of the various temporal discretizations w.r.t. the resulting accuracy for prototypical flow configurations of benchmarking character, we perform detailed simulations of two different nonstationary flow problems. The first test problem considers the classical 'flow around cylinder' configuration in [4]: Here, we concentrate on the nonstationary behavior of the flow patterns with periodic oscillations and examine the ability of the different time discretization schemes to capture the dynamics of the flow. The quantities of interest are the lift and drag coefficient, as well as the pressure drop between two points on the cylinder. The temporal accuracy is compared by means of plotting these physical quantities for various time step sizes and schemes,

DOI: 10.1002/fld

and particularly the deviation per cycle (in percentage) of the corresponding reference curves is of interest.

As a main result, the numerical tests show that the cGP(2)-method gains the same accuracy at time step sizes which are approximately 10 times larger than the associated time steps for cGP(1), resp., Crank-Nicolson (CN) while the dG(1)-method achieves this accuracy for which the associated time step is approximately 5 time larger than that of cGP(1) or CN. These tests have been performed for different spatial mesh levels and demonstrate the same grid-independent behaviour for all levels.

As a second test problem, we analyze the nonstationary 'flow through a Venturi pipe' which can be found as a small device in sailing boats: If the inflow speed from the inlet is sufficiently large, then due to the Bernoulli principle, the narrow section in the middle of the pipe produces a lower pressure which creates a flux through the upper part of the small pipe. One of the objectives of this simulation is to control the instantaneous and mean flux through this device (see also [5, 6]). In order to compare the different temporal discretizations, the flow is always started from a same start solution (namely the Stokes solution) and the simulations are performed for 30 time units with various time step sizes. Again, the numerical results demonstrate that the necessary time step sizes for cGP(2), for which almost the same results are obtained as for cGP(1) or CN, are 10 times larger while for the dG(1) approach they are 5 times larger. These factors 10 and 5 become even more clear for higher space mesh levels when more and more scales of this complex flow configuration can be resolved. As a main conclusion, we can say that the presented cGP(2) approach, together with special Newton-multigrid FEM solvers which can handle large time steps and large problem sizes in a very efficient way, has a great potential for complex flow simulations due to its high accuracy and robustness.

The paper is organized as follows: Section 2 describes the theoretical details of *continuous* Galerkin-Petrov (cGP(k)) and *discontinuous* Galerkin (dG(k)) methods. The finite element space discretization is considered in Section 3 together with the resulting discrete problems. Finally, Section 4 presents the numerical results for a couple of test problems. In Section 5, the paper is concluded with a discussion of the results.

2. GALERKIN TIME STEPPING FOR THE NAVIER-STOKES EQUATIONS

For a domain $\Omega \subset \mathbb{R}^d$, we consider the nonstationary incompressible Navier-Stokes equations, i.e. we want to find for each time $t \in [0,T]$ a velocity field $\mathbf{u}(t) : \Omega \to \mathbb{R}^d$ and a pressure field $p(t) : \Omega \to \mathbb{R}$ *such that*

$$\begin{array}{rcll} \partial_t \mathbf{u} - \nu \triangle \mathbf{u} + (\mathbf{u} \cdot \nabla)\mathbf{u} + \nabla p & = & f, & \text{in} \quad \Omega \times (0,T], \\ \text{div}\, \mathbf{u} & = & 0 & \text{in} \quad \Omega \times (0,T], \\ \mathbf{u} & = & g & \text{on} \quad \partial\Omega \times (0,T], \\ \mathbf{u}(x,0) & = & \mathbf{u}_0(x) & \text{in} \quad \Omega \quad \text{for} \quad t = 0, \end{array} \tag{1}$$

where ν denotes the viscosity, f the body force and $\mathbf{u}_0$ the initial velocity field at time $t = 0$. For simplicity, we restrict to the case $d = 2$ and we assume homogeneous Dirichlet conditions at the boundary $\partial\Omega$ of a polygonal domain Ω (for other choices see [8]). To make this problem well-posed in the case of pure Dirichlet boundary conditions, we have to look for the field $p(t)$ at each time t in the subspace $L^2_0(\Omega) \subset L^2(\Omega)$ of functions with zero integral mean value.

DOI: 10.1002/fld

For the time discretization, we decompose the time interval $I = (0, T]$ into N disjoint subintervals $I_n := (t_{n-1}, t_n]$, where $n = 1, \ldots, N$ and $0 = t_0 < t_1 < \cdots < t_{N-1} < t_N = T$. Thus, the value of the time-discrete approximation $\mathbf{u}_\tau$ at time t_n is always defined as the I_n-value (i.e. the left-sided value in case of discontinuous approximation) $\mathbf{u}_\tau(t_n) := \mathbf{u}^- := \mathbf{u}_\tau|_{I_n}(t_n)$. The symbol τ denotes the *time discretization parameter* and is also used as the maximum time step size $\tau := \max_{1\le n\le N} \tau_n$, where $\tau_n := t_n - t_{n-1}$. Then, for the subsequent continuous and discontinuous Galerkin time stepping schemes, we approximate the solution $\mathbf{u}$ by means of a function $\mathbf{u}_\tau$ which is piecewise polynomial with respect to time. In case of the cGP(k)-method, we are looking for $\mathbf{u}_\tau$ in the discrete time-continuous space (with $\mathbf{V} = (H_0^1(\Omega))^2$)

$$\mathbf{X}_\tau^k := \{\mathbf{u} \in C(I, \mathbf{V}) : \ \mathbf{u}\big|_{I_n} \in \mathbb{P}_k(I_n, \mathbf{V}) \quad \forall\, n = 1, \ldots, N\}, \tag{2}$$

where

$$\mathbb{P}_k(I_n, \mathbf{V}) := \Big\{\mathbf{u} : I_n \to \mathbf{V} \ : \ \mathbf{u}(t) = \sum_{j=0}^{k} \mathbf{U}^j t^j \ , \ \forall\, t \in I_n, \ \mathbf{U}^j \in \mathbf{V}, \ \forall\, j\Big\}. \tag{3}$$

Moreover, we introduce the discrete time-discontinuous test space

$$\mathbf{Y}_\tau^{k-1} := \{\mathbf{v} \in L^2(I, \mathbf{V}) : \ \mathbf{v}\big|_{I_n} \in \mathbb{P}_{k-1}(I_n, \mathbf{V}) \quad \forall\, n = 1, \ldots, N\} \tag{4}$$

consisting of piecewise polynomials of order $k-1$ which are (globally) discontinuous at the end points of the time intervals. Similarly, we will use for the time-discrete pressure p_τ an analogous ansatz space $\tilde{X}_\tau^k$, where the vector valued space $\mathbf{V}$ is replaced by the scalar valued space $Q = L_0^2(\Omega)$, and an analogous discontinuous test space $\tilde{Y}_\tau^{k-1}$.

In case of the dG($k-1$)-method, we are looking for $\mathbf{u}_\tau$ in the time-discontinuous discrete space $\mathbf{Y}_\tau^{k-1}$. Next, we describe separately the cGP(k) and dG($k-1$)-method.

2.1. cGP(k)-method

In order to derive the time discretization, we multiply the equations in (1) with some suitable I_n-supported test functions and integrate over $\Omega \times I_n$. To determine $\mathbf{u}_\tau|_{I_n}$ and $p_\tau|_{I_n}$ we represent them by the polynomial ansatz

$$\mathbf{u}_\tau|_{I_n}(t) := \sum_{j=0}^{k} \mathbf{U}_n^j \phi_{n,j}(t), \qquad p_\tau|_{I_n}(t) := \sum_{j=0}^{k} P_n^j \phi_{n,j}(t), \tag{5}$$

where the "coefficients" $(\mathbf{U}_n^j, P_n^j)$ are elements of the function spaces $\mathbf{V} \times Q$ and the polynomial functions $\phi_{n,j} \in \mathbb{P}_k(I_n)$ are the Lagrange basis functions with respect to the $k+1$ nodal points $t_{n,j} \in I_n$ satisfying the conditions

$$\phi_{n,j}(t_{n,i}) = \delta_{i,j}, \qquad i, j = 0, \ldots, k \tag{6}$$

with the Kronecker symbol $\delta_{i,j}$. For an easy treatment of the initial condition, we set $t_{n,0} = t_{n-1}$. Then, the initial condition is equivalent to the condition

$$\mathbf{U}_n^0 = \mathbf{u}_\tau|_{I_{n-1}}(t_{n-1}) \quad \text{if} \quad n \ge 2 \qquad \text{or} \qquad \mathbf{U}_n^0 = \mathbf{u}_0 \quad \text{if} \quad n = 1. \tag{7}$$

The other points $t_{n,1}, \ldots, t_{n,k}$ are chosen as the quadrature points of the k-point Gaussian formula on I_n which is exact if the function to be integrated is a polynomial of degree less or equal to $2k-1$. We define the basis functions $\phi_{n,j} \in \mathbb{P}_k(I_n)$ of (5) via affine reference transformations (see [1, 2]

DOI: 10.1002/fld

for more details). Now, we can describe the *time discrete I_n-problem of the cGP(k)-method* [1, 9]:

Find on the interval $I_n = (t_{n-1}, t_n]$ the k unknown pairs of "coefficients" $(\mathbf{U}_n^j, P_n^j) \in \mathbf{V} \times Q$, $j = 1, \dots, k$, such that for all $i = 1, \dots, k$, it holds for all $(\mathbf{v}, q) \in \mathbf{V} \times Q$

$$\begin{aligned} \sum_{j=0}^{k} \alpha_{i,j} \left(\mathbf{U}_n^j, \mathbf{v}\right)_\Omega + \frac{\tau_n}{2} a(\mathbf{U}_n^i, \mathbf{v}) + \frac{\tau_n}{2} n(\mathbf{U}_n^i, \mathbf{U}_n^i, \mathbf{v}) + \frac{\tau_n}{2} b(\mathbf{v}, P_n^i) &= \tfrac{\tau_n}{2} \left(f(t_{n,i}), \mathbf{v}\right)_\Omega \\ b(\mathbf{U}_n^i, q) &= 0 \end{aligned} \tag{8}$$

with $\mathbf{U}_n^0 := \mathbf{u}_\tau(t_{n-1})$ for $n > 1$, $\mathbf{U}_1^0 := \mathbf{u}_0$ and $(\cdot, \cdot)_\Omega$ denotes the usual inner product in $(L^2(\Omega))^d$. The bilinear forms $a(\cdot, \cdot)$ and $b(\cdot, \cdot)$ on $\mathbf{V} \times \mathbf{V}$ and $\mathbf{V} \times Q$, respectively, are defined as

$$a(\mathbf{u}, \mathbf{v}) := \int_\Omega \nabla \mathbf{u} \cdot \nabla \mathbf{v} \, dx \quad \forall\, \mathbf{u}, \mathbf{v} \in \mathbf{V}, \qquad b(\mathbf{v}, p) := -\int_\Omega \nabla \cdot \mathbf{v} \, p \, dx, \tag{9}$$

and the trilinear form $n(\cdot, \cdot, \cdot)$ on $\mathbf{V} \times \mathbf{V} \times \mathbf{V}$ is given as $n(\mathbf{w}, \mathbf{u}, \mathbf{v}) := \sum_{i=1}^d n_i(\mathbf{w}, u_i, v_i)$ where

$$n_i(\mathbf{w}, u_i, v_i) := \int_\Omega (\mathbf{w} \cdot \nabla u_i) v_i \, dx \quad \forall\, \mathbf{w} \in \mathbf{V}, \quad u_i, v_i \in H_0^1(\Omega). \tag{10}$$

A typical property of this cGP(k)-variant is that the initial pressure P_n^0 of the ansatz (5) does not occur in this formulation. In order to achieve superconvergence for the pressure approximation at the discrete time levels t_n special interpolation techniques using two neighboured time intervals can be applied (see [2]).

In the following subsections, we specify the constants $\alpha_{i,j}$ of the cGP(k)-method for the cases $k = 1$ and $k = 2$, and for comparison we describe explicitly the well-known dG(1) approach (see [2] for more details).

2.1.1. cGP(1)-method. We use the one-point Gaussian quadrature formula with $\hat{t}_1 = 0$ and $t_{n,1} = t_{n-1} + \frac{\tau_n}{2}$. Then, we get $\alpha_{1,0} = -1$ and $\alpha_{1,1} = 1$ (see [1, 2]). Thus, problem (8) leads to the following problem for the "one" pair of unknowns $\mathbf{U}_n^1 = \mathbf{u}_\tau(t_{n-1} + \frac{\tau_n}{2})$ and $P_n^1 = p_\tau(t_{n-1} + \frac{\tau_n}{2})$: Find $(\mathbf{U}_n^1, P_n^1) \in \mathbf{V} \times Q$ such that for all $(\mathbf{v}, q) \in \mathbf{V} \times Q$ it holds

$$\begin{aligned} \left(\mathbf{U}_n^1, \mathbf{v}\right)_\Omega + \tfrac{\tau_n}{2} a(\mathbf{U}_n^1, \mathbf{v}) + \tfrac{\tau_n}{2} n(\mathbf{U}_n^1, \mathbf{U}_n^1, \mathbf{v}) + \tfrac{\tau_n}{2} b(\mathbf{v}, P_n^1) &= \tfrac{\tau_n}{2} \left(f(t_{n,1}), \mathbf{v}\right)_\Omega + \left(\mathbf{U}_n^0, \mathbf{v}\right)_\Omega \\ b(\mathbf{U}_n^1, q) &= 0. \end{aligned} \tag{11}$$

Once we have determined the solution $\mathbf{U}_n^1$ at the midpoint $t_{n,1}$ of the time interval I_n, we get the solution at the next discrete time point t_n simply by linear extrapolation based on the ansatz (5), i.e.,

$$\mathbf{u}_\tau(t_n) = 2\mathbf{U}_n^1 - \mathbf{U}_n^0, \tag{12}$$

where $\mathbf{U}_n^0$ is the initial value at the time interval $(t_{n-1}, t_n]$ coming from the previous time interval I_{n-1} or the initial value $\mathbf{u}_0$.

If we would replace $f(t_{n,1})$ by the mean value $(f(t_{n-1}) + f(t_n))/2$, which means that we replace the one-point Gaussian quadrature of the right hand side by the trapezoidal rule, the resulting cGP(1)-method is equivalent to the well-known *Crank-Nicolson scheme*. The cGP(1)-method is accurate of order 2 in the whole time interval as it is known for the Crank-Nicolson scheme. Concerning the pressure approximation, one observes that the second order accuracy holds only in the midpoints of the time intervals. By means of linear interpolation between the midpoints of two neighbouring time intervals we get second order accuracy also at the discrete time levels t_n.

DOI: 10.1002/fld

2.1.2. cGP(2)-method. Here, we use the 2-point Gaussian quadrature formula with the points $\hat{t}_1 = -\frac{1}{\sqrt{3}}$ and $\hat{t}_2 = \frac{1}{\sqrt{3}}$. Then, we obtain the coefficients

$$(\alpha_{i,j}) = \begin{pmatrix} -\sqrt{3} & \frac{3}{2} & \frac{2\sqrt{3}-3}{2} \\ \sqrt{3} & \frac{-2\sqrt{3}-3}{2} & \frac{3}{2} \end{pmatrix} \qquad i = 1,2,\ j = 0,1,2. \tag{13}$$

Consequently, on the time interval I_n, we have to solve for the two "unknowns"

$$(\mathbf{U}_n^j, P_n^j) = \big(\mathbf{u}_\tau(t_{n,j}), p_\tau(t_{n,j})\big) \in \mathbf{V} \times Q \qquad \text{with} \qquad t_{n,j} := (t_{n-1} + t_n + \tau_n \hat{t}_j)/2 \quad \text{for} \quad j = 1,2. \tag{14}$$

The corresponding coupled system reads

$$\begin{aligned} \alpha_{1,1}\left(\mathbf{U}_n^1, \mathbf{v}\right)_\Omega + \tfrac{\tau_n}{2} a(\mathbf{U}_n^1, \mathbf{v}) + \tfrac{\tau_n}{2} n(\mathbf{U}_n^1, \mathbf{U}_n^1, \mathbf{v}) + \alpha_{1,2}\left(\mathbf{U}_n^2, \mathbf{v}\right)_\Omega + \tfrac{\tau_n}{2} b(\mathbf{v}, P_n^1) &= \ell_1(\mathbf{v}) \\ \alpha_{2,1}\left(\mathbf{U}_n^1, \mathbf{v}\right)_\Omega + \alpha_{2,2}\left(\mathbf{U}_n^2, \mathbf{v}\right)_\Omega + \tfrac{\tau_n}{2} a(\mathbf{U}_n^2, \mathbf{v}) + \tfrac{\tau_n}{2} n(\mathbf{U}_n^2, \mathbf{U}_n^2, \mathbf{v}) + \tfrac{\tau_n}{2} b(\mathbf{v}, P_n^2) &= \ell_2(\mathbf{v}) \\ b(\mathbf{U}_n^1, q) &= 0 \\ b(\mathbf{U}_n^2, q) &= 0, \end{aligned} \tag{15}$$

which has to be satisfied for all $(\mathbf{v}, q) \in \mathbf{V} \times Q$ with

$$\ell_i(\mathbf{v}) = \frac{\tau_n}{2}\left(f(t_{n,i}), \mathbf{v}\right)_\Omega - \alpha_{i,0}\left(\mathbf{U}_n^0, \mathbf{v}\right)_\Omega \qquad i = 1,2. \tag{16}$$

Once we have determined the solutions $\mathbf{U}_n^1$, $\mathbf{U}_n^2$ at the Gaussian points in the interior of the interval I_n, we get the solution at the right boundary t_n of I_n by means of quadratic extrapolation from the ansatz (5), i.e.,

$$\mathbf{u}_\tau(t_n) = \mathbf{U}_n^0 + \sqrt{3}(\mathbf{U}_n^2 - \mathbf{U}_n^1), \tag{17}$$

where $\mathbf{U}_n^0$ is the initial value at the time interval I_n. The cGP(2)-method is accurate of order 3 in the whole time interval and superconvergent of order 4 in the discrete time points (see [1, 2]).

2.2. *dG($k-1$)-method*

Here, the time-discrete velocity and pressure solution is determined in the solution space $(\mathbf{u}_\tau, p_\tau) \in \mathbf{Y}_\tau^{k-1} \times \tilde{Y}_\tau^{k-1}$, where $k \geq 1$. The ansatz for $(\mathbf{u}_\tau, p_\tau)$ on interval I_n is then analog to (5) with the difference that the sum starts with $j = 1$ and the scalar basis functions $\phi_{n,j}$ are polynomials of order $k-1$. In this paper, we will concentrate only on the case $k = 2$, i.e. on the well-known dG(1)-method. We can derive the following constants for $i, j \in \{1, 2\}$ (see again [1] and [2])

$$(\alpha_{i,j}) = \begin{pmatrix} 1 & \frac{\sqrt{3}-1}{2} \\ \frac{-\sqrt{3}-1}{2} & 1 \end{pmatrix}, \quad (d_i) = \begin{pmatrix} \frac{\sqrt{3}+1}{2} \\ \frac{-\sqrt{3}+1}{2} \end{pmatrix}. \tag{18}$$

Then, on the time interval I_n, one has to determine the two "unknowns" $(\mathbf{U}_n^j, P_n^j) \in \mathbf{V} \times Q$ as the solution of the following coupled system

$$\begin{aligned} \alpha_{1,1}\left(\mathbf{U}_n^1, \mathbf{v}\right)_\Omega + \tfrac{\tau_n}{2} a(\mathbf{U}_n^1, \mathbf{v}) + \tfrac{\tau_n}{2} n(\mathbf{U}_n^1, \mathbf{U}_n^1, \mathbf{v}) + \tfrac{\tau_n}{2} b(\mathbf{v}, P_n^1) + \alpha_{1,2}\left(\mathbf{U}_n^2, \mathbf{v}\right)_\Omega &= \ell_1(\mathbf{v}) \\ \alpha_{2,1}\left(\mathbf{U}_n^1, \mathbf{v}\right)_\Omega + \alpha_{2,2}\left(\mathbf{U}_n^2, \mathbf{v}\right)_\Omega + \tfrac{\tau_n}{2} a(\mathbf{U}_n^2, \mathbf{v}) + \tfrac{\tau_n}{2} n(\mathbf{U}_n^2, \mathbf{U}_n^2, \mathbf{v}) + \tfrac{\tau_n}{2} b(\mathbf{v}, P_n^2) &= \ell_2(\mathbf{v}) \\ b(\mathbf{U}_n^1, q) &= 0 \\ b(\mathbf{U}_n^2, q) &= 0 \end{aligned} \tag{19}$$

which has to be satisfied for all $(\mathbf{v}, q) \in \mathbf{V} \times Q$ with $\ell_i(\cdot)$ defined by

$$\ell_i(\mathbf{v}) = \frac{\tau_n}{2}\left(f(t_{n,i}), \mathbf{v}\right)_\Omega + d_i\left(\mathbf{U}_n^0, \mathbf{v}\right)_\Omega \qquad i = 1,2. \tag{20}$$

DOI: 10.1002/fld

Once we have solved the above system, we obtain $\mathbf{u}_\tau$ and p_τ at the time t_n by means of the following linear extrapolation

$$\mathbf{u}_\tau(t_n) = \frac{\sqrt{3}+1}{2}\mathbf{U}_n^2 - \frac{\sqrt{3}-1}{2}\mathbf{U}_n^1 \qquad \text{and} \qquad p_\tau(t_n) = \frac{\sqrt{3}+1}{2}P_n^2 - \frac{\sqrt{3}-1}{2}P_n^1. \tag{21}$$

The dG(1)-method is of order 2 in the whole time interval and superconvergent of order 3 in the discrete time points (see [1, 2]).

3. SPACE DISCRETIZATION BY FEM

After discretizing the Navier-Stokes equations (1) in time, we now discretize the resulting "I_n-problems" in space by using the finite element method [10, 11, 12, 13]. In our numerical experiments, the finite element spaces $\mathbf{V}_h \subset \mathbf{V}$ and $Q_h \subset Q$ are defined by biquadratic and discontinuous linear finite elements, respectively, on a quadrilateral mesh T_h covering the computational domain Ω. Each "I_n-problem" for the cGP(k) or the dG($k-1$)-approach has the structure:

For given $\mathbf{U}_n^0 \in \mathbf{V}$, find $(\mathbf{U}_n^j, P_n^j) \in \mathbf{V} \times Q$, $j = 1, \ldots, k$, such that

$$\begin{aligned} \sum_{j=1}^{k} \alpha_{i,j} \left(\mathbf{U}_n^j, \mathbf{v}\right)_\Omega + \frac{\tau_n}{2} a(\mathbf{U}_n^i, \mathbf{v}) + \frac{\tau_n}{2} n(\mathbf{U}_n^i, \mathbf{U}_n^i, \mathbf{v}) + \frac{\tau_n}{2} b(\mathbf{v}, P_n^i) &= \ell_i(\mathbf{v}) \\ b(\mathbf{U}_n^i, q) &= 0, \end{aligned} \tag{22}$$

which has to be satisfied for all $i = 1, \ldots, k$ and all $(\mathbf{v}, q) \in \mathbf{V} \times Q$ with

$$\ell_i(\mathbf{v}) := \frac{\tau_n}{2} \left(f(t_{n,i}), \mathbf{v}\right)_\Omega + d_i \left(\mathbf{U}_n^0, \mathbf{v}\right)_\Omega \tag{23}$$

where $\alpha_{i,j}$ and d_i are the corresponding constants described above.

For the space discretization, all $(\mathbf{U}_n^j, P_n^j) \in \mathbf{V} \times Q$ are approximated by finite element functions $(\mathbf{U}_{n,h}^j, P_{n,h}^j) \in \mathbf{V}_h \times Q_h$, respectively, and the fully discrete "I_n-problem" reads:

For given $\mathbf{U}_{n,h}^0 \in \mathbf{V}_h$, find $(\mathbf{U}_{n,h}^j, P_{n,h}^j) \in \mathbf{V}_h \times Q_h$, $j = 1, \ldots, k$, such that it holds

$$\begin{aligned} \sum_{j=1}^{k} \alpha_{i,j} \left(\mathbf{U}_{n,h}^j, \mathbf{v}_h\right)_\Omega + \frac{\tau_n}{2} a(\mathbf{U}_{n,h}^i, \mathbf{v}_h) + \frac{\tau_n}{2} n(\mathbf{U}_{n,h}^i, \mathbf{U}_{n,h}^i, \mathbf{v}_h) + \frac{\tau_n}{2} b(\mathbf{v}_h, P_{n,h}^i) &= \ell_i(\mathbf{v}_h) \\ b(\mathbf{U}_{n,h}^i, q_h) &= 0 \end{aligned} \tag{24}$$

for all $(\mathbf{v}_h, q_h) \in \mathbf{V}_h \times Q_h$ and all $i = 1, \ldots, k$.

Once we have solved this system, we have computed for each time $t \in I_n$ a finite element approximation $u_{\tau,h}(t) \in \mathbf{V}_h$ of the time discrete solution $\mathbf{u}_\tau(t) \in \mathbf{V}$ which is defined by an analogous ansatz to (5) where the $\mathbf{U}_n^j \in \mathbf{V}$ are replaced by the discrete functions $\mathbf{U}_{n,h}^j \in \mathbf{V}_h$.

In the following, we will write problem (24) as a nonlinear algebraic block system. Let $S_h \subset H_0^1(\Omega)$ denote the scalar finite element space for the velocity components $U_n^j, V_n^j \in S_h$ of

DOI: 10.1002/fld

$\mathbf{U}_{n,h}^j = (U_{n,h}^j, V_{n,h}^j) \in \mathbf{V}_h = S_h^2$ and let $\phi_\mu \in S_h$, $\mu = 1, \ldots, m_h$, denote the scalar finite element basis functions of S_h. Then, we define the nodal vector $\underline{\mathbf{U}}_n^j = (\underline{U}_n^j, \underline{V}_n^j) \in \mathbb{R}^{2m_h}$ of $\mathbf{U}_{n,h}^j = (U_{n,h}^j, V_{n,h}^j) \in \mathbf{V}_h$ such that

$$U_{n,h}^j(x) = \sum_{\mu=1}^{m_h} (\underline{U}_n^j)_\mu \phi_\mu(x), \qquad V_{n,h}^j(x) = \sum_{\mu=1}^{m_h} (\underline{V}_n^j)_\mu \phi_\mu(x) \qquad \forall\, x \in \Omega. \tag{25}$$

Similarly for the pressure, let $\psi_\mu \in Q_h$, $\mu = 1, \ldots, n_h$, denote the finite element basis functions and $\underline{P}_n^j \in \mathbb{R}^{n_h}$ the nodal vector of $P_{n,h}^j \in Q_h$ such that

$$P_{n,h}^j(x) = \sum_{\mu=1}^{n_h} (\underline{P}_n^j)_\mu \psi_\mu(x) \qquad \forall\, x \in \Omega. \tag{26}$$

Furthermore, we introduce the mass matrix $M \in \mathbb{R}^{m_h \times m_h}$, the discrete Laplacian matrix $L \in \mathbb{R}^{m_h \times m_h}$, the gradient matrices $B_i \in \mathbb{R}^{n_h \times m_h}$, $i = 1, 2$, as

$$M_{\nu,\mu} := (\phi_\mu, \phi_\nu)_\Omega\,, \quad L_{\nu,\mu} := a(\phi_\mu, \phi_\nu), \quad (B_i)_{\nu,\mu} := b(\phi_\mu \mathbf{e}^i, \psi_\nu), \tag{27}$$

and the right hand side vectors $F_n^i, G_n^i \in \mathbb{R}^{m_h}$, $i = 1, \ldots, k$, with the components

$$(F_n^i)_\nu := \left(f(t_{n,i}), \phi_\nu \mathbf{e}^1\right)_\Omega, \quad (G_n^i)_\nu := \left(f(t_{n,i}), \phi_\nu \mathbf{e}^2\right)_\Omega. \tag{28}$$

Next, for a given discrete velocity field $\mathbf{w}_h \in \mathbf{V}_h$ with the nodal vector $\underline{\mathbf{w}} \in \mathbb{R}^{2m_h}$, we define the matrix $N(\underline{\mathbf{w}}) \in \mathbb{R}^{m_h \times m_h}$ as

$$N(\underline{\mathbf{w}})_{\nu,\mu} := n(\mathbf{w}_h, \phi_\mu, \phi_\nu). \tag{29}$$

Using the block-matrices and block-vectors

$$\mathbf{M} = \begin{bmatrix} M & 0 \\ 0 & M \end{bmatrix}, \quad \mathbf{L} = \begin{bmatrix} L & 0 \\ 0 & L \end{bmatrix}, \quad \mathbf{N}(\underline{\mathbf{w}}) = \begin{bmatrix} N(\underline{\mathbf{w}}) & 0 \\ 0 & N(\underline{\mathbf{w}}) \end{bmatrix}, \quad \mathbf{B} = \begin{bmatrix} B_1 \\ B_2 \end{bmatrix}, \quad \mathbf{F}_n^i = \begin{bmatrix} F_n^i \\ G_n^i \end{bmatrix}, \tag{30}$$

the fully discrete "I_n-problem" is equivalent to the following nonlinear $k \times k$ block system:

For given $\underline{\mathbf{U}}_n^0 \in \mathbb{R}^{2m_h}$, *find* $\underline{\mathbf{U}}_n^j \in \mathbb{R}^{2m_h}$ *and* $\underline{P}_n^j \in \mathbb{R}^{n_h}$, $j = 1, \ldots, k$, *such that for all* $i = 1, \ldots, k$, *it holds*

$$\begin{aligned} \sum_{j=1}^{k} \alpha_{i,j} \mathbf{M} \underline{\mathbf{U}}_n^j + \frac{\tau_n}{2} \mathbf{L} \underline{\mathbf{U}}_n^i + \frac{\tau_n}{2} \mathbf{N}(\underline{\mathbf{U}}_n^i) \underline{\mathbf{U}}_n^i + \frac{\tau_n}{2} \mathbf{B} \underline{P}_n^i \quad &= \quad d_i \mathbf{M} \underline{\mathbf{U}}_n^0 + \tfrac{\tau_n}{2} \mathbf{F}_n^i, \\ \mathbf{B}^T \underline{\mathbf{U}}_n^i \quad &= \quad 0. \end{aligned} \tag{31}$$

The vector $\underline{\mathbf{U}}_n^0$ is defined as the finite element nodal vector of the fully discrete solution $\mathbf{u}_{\tau,h}(t_{n-1})$ computed from the previous time interval $[t_{n-2}, t_{n-1}]$ if $n \geq 2$ or from a finite element interpolation of the initial data $\mathbf{u}_0$ if $n = 1$. In the case of higher Reynolds numbers, we apply additionally an edge oriented FEM stabilization (EOFEM) [14] for the convective term. This means that we replace the trilinear form $n(\mathbf{w}, \cdot, \cdot)$ by a modified form $n_h(\mathbf{w}, \cdot, \cdot)$ such that, in (31), differences will appear only in the nonlinear matrix $\mathbf{N}(\underline{\mathbf{w}})$.

In the following, we will present the resulting block systems for the cGP(1), cGP(2) and dG(1) method which are used in our numerical experiments.

DOI: 10.1002/fld

3.1. cGP(1)-method

The problem on time interval I_n reads:

For given initial velocity $\underline{\mathbf{U}}_n^0 = (\underline{U}_n^0, \underline{V}_n^0)$*, find* $\underline{\mathbf{U}}_n^1 = (\underline{U}_n^1, \underline{V}_n^1)$ *and a pressure* $\underline{P}_n^1$ *such that*

$$\begin{aligned}\left(M + \tfrac{\tau_n}{2}L + \tfrac{\tau_n}{2}N_1\right)\underline{U}_n^1 + \tfrac{\tau_n}{2}B_1\underline{P}_n^1 &= \tfrac{\tau_n}{2}F_n^1 + M\underline{U}_n^0 \\ \left(M + \tfrac{\tau_n}{2}L + \tfrac{\tau_n}{2}N_1\right)\underline{V}_n^1 + \tfrac{\tau_n}{2}B_2\underline{P}_n^1 &= \tfrac{\tau_n}{2}G_n^1 + M\underline{V}_n^0 \\ B_1^T\underline{U}_n^1 + B_2^T\underline{V}_n^1 &= 0\end{aligned} \tag{32}$$

where $N_1 := N(\underline{\mathbf{w}}^1)$ with $\underline{\mathbf{w}}^1 := (\underline{U}_n^1, \underline{V}_n^1)^T$ denotes the nonlinear convection operator. Once we have determined the solution $\underline{U}_n^1$, $\underline{V}_n^1$ we compute the nodal vector $\underline{U}_{n+1}^0$, $\underline{V}_{n+1}^0$ of the fully discrete solution $\mathbf{u}_{\tau,h}$ at time t_n by using the following linear extrapolation

$$u_{\tau,h}(t_n) \sim \underline{U}_{n+1}^0 = 2\underline{U}_n^1 - \underline{U}_n^0, \qquad v_{\tau,h}(t_n) \sim \underline{V}_{n+1}^0 = 2\underline{V}_n^1 - \underline{V}_n^0. \tag{33}$$

3.2. cGP(2)-method

The 6×6 block system on time interval I_n reads:

For given initial velocity $\underline{\mathbf{U}}_n^0 = (\underline{U}_n^0, \underline{V}_n^0)$*, find* $\underline{U}_n^1, \underline{U}_n^2, \underline{V}_n^1, \underline{V}_n^2$ *and* $\underline{P}_n^1, \underline{P}_n^2$ *such that*

$$\begin{aligned}(3M + \tau_n L + \tau_n N_1)\underline{U}_n^1 + \left(2\sqrt{3} - 3\right)M\underline{U}_n^2 + \tau_n B_1\underline{P}_n^1 &= \tau_n F_n^1 + 2\sqrt{3}M\underline{U}_n^0 \\ \left(-2\sqrt{3} - 3\right)M\underline{U}_n^1 + (3M + \tau_n L + \tau_n N_2)\underline{U}_n^2 + \tau_n B_1\underline{P}_n^2 &= \tau_n F_n^2 - 2\sqrt{3}M\underline{U}_n^0 \\ (3M + \tau_n L + \tau_n N_1)\underline{V}_n^1 + \left(2\sqrt{3} - 3\right)M\underline{V}_n^2 + \tau_n B_2\underline{P}_n^1 &= \tau_n G_n^1 + 2\sqrt{3}M\underline{V}_n^0 \\ \left(-2\sqrt{3} - 3\right)M\underline{V}_n^1 + (3M + \tau_n L + \tau_n N_2)\underline{V}_n^2 + \tau_n B_2\underline{P}_n^2 &= \tau_n G_n^2 - 2\sqrt{3}M\underline{V}_n^0 \\ B_1^T\underline{U}_n^1 + B_2^T\underline{V}_n^1 &= 0 \\ B_1^T\underline{U}_n^2 + B_2^T\underline{V}_n^2 &= 0\end{aligned} \tag{34}$$

where $N_i := N(\underline{\mathbf{w}}^i)$ with $\underline{\mathbf{w}}^i = (\underline{U}_n^i, \underline{V}_n^i)^T$, $i = 1, 2$, denotes the nonlinear convection operator associated with the velocity approximation evaluated at the i-th Gauß point on the time interval. Once we have determined the solution $(\underline{U}_n^1, \underline{U}_n^2, \underline{V}_n^1, \underline{V}_n^2)$, we compute the nodal vectors $\underline{U}_{n+1}^0$ and $\underline{V}_{n+1}^0$ of the fully discrete solution $\mathbf{u}_{\tau,h}$ at time t_n by using the following quadratic extrapolation

$$u_{\tau,h}(t_n) \sim \underline{U}_{n+1}^0 = \underline{U}_n^0 + \sqrt{3}(\underline{U}_n^2 - \underline{U}_n^1), \qquad v_{\tau,h}(t_n) \sim \underline{V}_{n+1}^0 = \underline{V}_n^0 + \sqrt{3}(\underline{V}_n^2 - \underline{V}_n^1). \tag{35}$$

To get a higher order pressure at time t_n, particularly for the computation of lift, drag, etc., we perform a special post processing as described in [2].

3.3. dG(1)-method

The analogous 6×6 block system on the time interval I_n reads:

DOI: 10.1002/fld

For given initial velocity $\underline{\mathbf{U}}_n^0 = (\underline{U}_n^0, \underline{V}_n^0)$, *find* $\underline{U}_n^1, \underline{U}_n^2, \underline{V}_n^1, \underline{V}_n^2$ *and* $\underline{P}_n^1, \underline{P}_n^2$ *such that*

$$\begin{aligned}
(2M + \tau_n L + \tau_n N_1)\,\underline{U}_n^1 + \left(\sqrt{3}-1\right) M\underline{U}_n^2 + \tau_n B_1 \underline{P}_n^1 &= \tau_n F_n^1 + \left(\sqrt{3}+1\right) M\underline{U}_n^0 \\
\left(-\sqrt{3}-1\right) M\underline{U}_n^1 + (2M + \tau_n L + \tau_n N_2)\,\underline{U}_n^2 + \tau_n B_1 \underline{P}_n^2 &= \tau_n F_n^2 + \left(-\sqrt{3}+1\right) M\underline{U}_n^0 \\
(2M + \tau_n L + \tau_n N_1)\,\underline{V}_n^1 + \left(\sqrt{3}-1\right) M\underline{V}_n^2 + \tau_n B_2 \underline{P}_n^1 &= \tau_n G_n^1 + \left(\sqrt{3}+1\right) M\underline{V}_n^0 \\
\left(-\sqrt{3}-1\right) M\underline{V}_n^1 + (2M + \tau_n L + \tau_n N_2)\,\underline{V}_n^2 + \tau_n B_2 \underline{P}_n^2 &= \tau_n G_n^2 + \left(-\sqrt{3}+1\right) M\underline{V}_n^0 \\
B_1^T \underline{U}_n^1 + B_2^T \underline{V}_n^1 &= 0 \\
B_1^T \underline{U}_n^2 + B_2^T \underline{V}_n^2 &= 0
\end{aligned} \tag{36}$$

where again $N_i := N(\underline{\mathbf{w}}^i)$ with $\underline{\mathbf{w}}^i = (\underline{U}_n^i, \underline{V}_n^i)^T$, $i = 1, 2$, denotes the nonlinear convection operator associated with the velocity approximation evaluated at the i-th Gauß point on the time interval. Once we have determined the solution $(\underline{U}_n^1, \underline{U}_n^2, \underline{V}_n^1, \underline{V}_n^2)$, we compute the nodal vectors $\underline{U}_{n+1}^0$,$\underline{V}_{n+1}^0$ and $\underline{P}_{n+1}^0$ as the left side limit of the fully discrete solution $\mathbf{u}_{\tau,h}$ and $p_{\tau,h}$ at time t_n by using the following linear extrapolation

$$\begin{aligned}
u_{\tau,h}^-(t_n) \sim \underline{U}_{n+1}^0 &= \tfrac{\sqrt{3}+1}{2}\underline{U}_n^2 - \tfrac{\sqrt{3}-1}{2}\underline{U}_n^1, \\
v_{\tau,h}^-(t_n) \sim \underline{V}_{n+1}^0 &= \tfrac{\sqrt{3}+1}{2}\underline{V}_n^2 - \tfrac{\sqrt{3}-1}{2}\underline{V}_n^1, \\
p_{\tau,h}^-(t_n) \sim \underline{P}_{n+1}^0 &= \tfrac{\sqrt{3}+1}{2}\underline{P}_n^2 - \tfrac{\sqrt{3}-1}{2}\underline{P}_n^1.
\end{aligned} \tag{37}$$

The resulting nonlinear saddle point problems from (32), (34) or (36) are solved by using a Newton-multigrid method with Vanka type smoothers (see [2] for details). A detailed analysis regarding the solver behavior (similar to [3]) will be part of the forthcoming paper in [15]. The solution approach is based on an outer nonlinear loop which has to solve a linear system in each nonlinear step. The associated linear subproblems are solved by means of a geometrical multigrid method with a local pressure Schur complement smoother (see [5, 16, 3, 17]), resp., Vanka-like smoother. The corresponding linear systems in each time interval $(t_{n-1}, t_n]$, are 6×6 block systems in the case of the cGP(2) and dG(1) approach, and 3×3 block systems for the cGP(1)-method, respectively, as described before.

4. NUMERICAL RESULTS

Analytical test cases to analyze the order of convergence have been considered in [2]. Here, we perform nonstationary simulations for more complex flow configurations to demonstrate the temporal accuracy and efficiency of the presented higher order time discretization schemes for prototypical test cases of benchmarking character. To this end, we continue the work which had been started by one of the authors in [6], where different time stepping schemes for two problems, namely *flow around cylinder* and *flow through a Venturi pipe*, were analyzed. First, we consider the *flow around cylinder* configuration which has been described in [4]. Here, we will concentrate only on the nonstationary behavior of the flow patterns with periodic oscillations and examine the ability of the different time discretization schemes (combined with the same FEM discretization in space) to capture the dynamics of the flow.

As a second test case, we consider the nonstationary behavior of a higher Reynolds number flow through a Venturi pipe which has many real life and industrial applications. If the inflow speed from the inlet is sufficiently high, then due to the Bernoulli principle, the narrow section in the middle of the pipe produces a low pressure which creates a flux through the upper part of the small pipe. The objective of this simulation is to control the instantaneous and mean flux through this device.

4.1. Nonstationary flow around cylinder

The flow problem related to the 'flow around cylinder' configuration [4] is characterized as follows:

- (laminar) nonstationary Navier-Stokes equations at $Re = 100$
- parabolic inflow with $U_{\max} = 1.5$
- time interval: $[t_0, t_0 + T] = [0, 10]$, where t_0 corresponds to the fully developed solution for each mesh level
- space-discretization: Q_2-elements for velocity and discontinuous P_1-elements for the pressure on a quadrilateral mesh (Q_2/P_1^{disc})
- time-discretization: cGP(1), cGP(2), dG(1)
- no stabilization for space-discretization

Here, the domain Ω consists of a channel of height $H = 0.41$ and length $L = 2.2$ having a circular cylinder located at $(0.2, 0.2)$ with diameter $D = 0.1$, placed at right angle to the direction of the fluid (see Figure 1). Further details regarding the settings can be found on `http://www.featflow.de/en/benchmarks/cfdbenchmarking.html`.

The maximum velocity $U_{max} = 1.5$ yields $Re = 100$ which leads to periodically oscillatory time-dependent vortex shedding behind the cylinder. For this range of *Reynolds numbers* together with the Q_2/P_1^{disc} discretization, our results have shown that there is no need for stabilization of the convective terms.

Quantities of physical interest: The examined accuracy of the benchmark crucially depends on the following quantities computed on the boundary S of the cylinder

$$F_D = \int_S (\rho\nu \frac{\partial u_t}{\partial n} n_y - p n_x) dS, \quad \text{and particularly} \quad F_L = -\int_S (\rho\nu \frac{\partial u_t}{\partial n} n_x + p n_y) dS \tag{38}$$

representing the total forces in the horizontal and vertical directions, respectively. The resulting drag and lift coefficients are (with $\rho = 1$ and $U_{max} = 1.5$)

$$C_D = \frac{2F_D}{\rho U_{mean}^2 D}, \qquad C_L = \frac{2F_L}{\rho U_{mean}^2 D}. \tag{39}$$

Furthermore, the pressure drop on the cylinder which is defined as

$$\Delta p = p_A - p_B, \tag{40}$$

where $A(0.15, 0.2)$ and $B(0.25, 0.2)$ are points on the boundary of the cylinder, is also of interest. Beside these quantities, we also compare the accuracy of the different time discretization schemes by computing the v velocity at the point $P(0.4, 0.2)$ near the obstacle.

Figure 2 shows the initial coarse mesh (level 1), which will be uniformly refined, and Figure 3 presents for different space mesh levels the number '#EL' of elements and the total number '#DOF'

DOI: 10.1002/fld

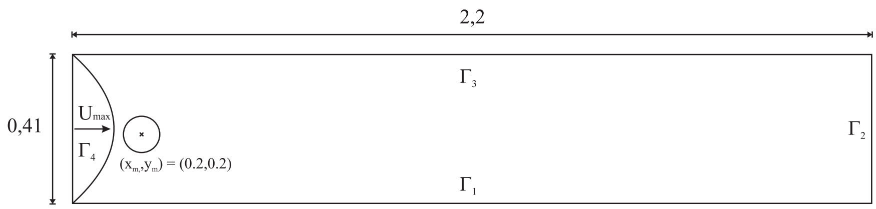

Figure 1. Geometry for the *flow around cylinder* configuration in 2D.

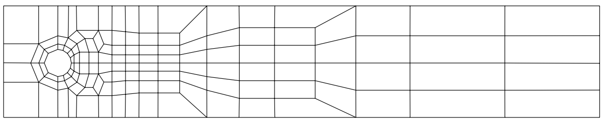

Figure 2. Coarse mesh for *flow around cylinder*.

Lev.	#EL	#DOF(total)
2	520	5 928
3	2 080	23 296
4	8 320	92 352

Figure 3. Size of the different systems in space.

of degrees of freedom where the finite element discretization is carried out by using the described biquadratic Q_2-element for velocity and discontinuous P_1-element for the pressure.

In order to compare the accuracy of the different time discretizations, the flow is started from a fully developed solution, that means the simulation on the same mesh with small time step had been performed until a fully periodical flow behavior had been reached, at time t_0, and the simulation is performed until T=10 using different time discretization methods for various uniform time step sizes $\tau_n := \tau$. After T=10, all the introduced quantities are plotted and analyzed in detail. To this end, in addition to the global picture of all quantities from time t_0 to $t_0 + 10$, these quantities are also zoomed in the last unit from T=9 to T=10. Since the results obtained from the Crank-Nicolson and cGP(1)-method are almost identical as expected, we show the results for the cGP(1) only together with the cGP(2) and dG(1)-method. All the time discretization schemes are started from the same initial solution (fully developed velocity field) and pressure and the simulations are performed with the same time step sizes. First, we show the results for mesh level 4. Next, we demonstrate that the results are already grid independent by showing them for different (space) levels for the cGP(2)-method, so that higher levels are not required.

DOI: 10.1002/fld

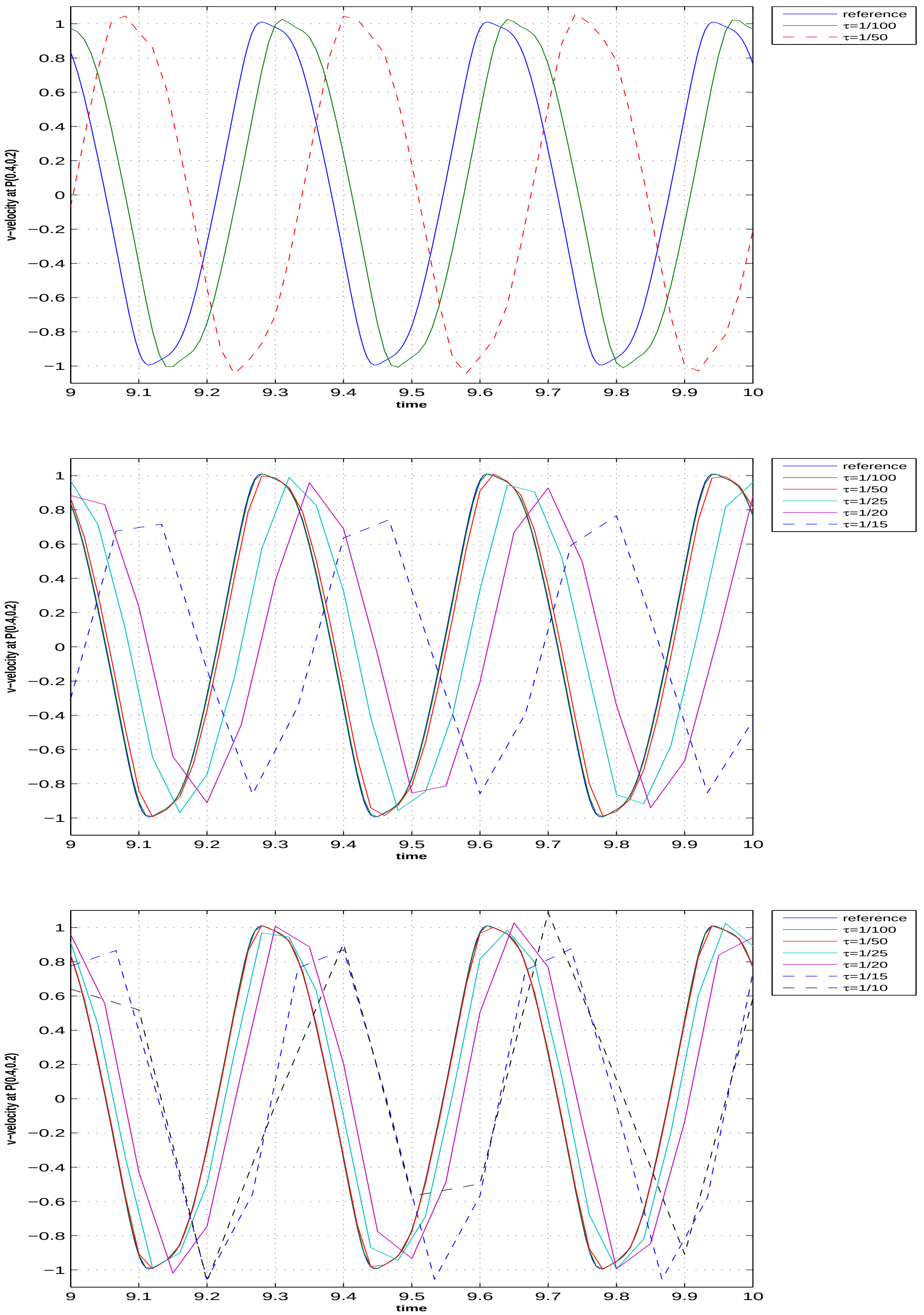

Figure 4. v-velocity at point $P(0.4, 0.2)$ for level 4 for different τ, using cGP(1) (top), dG(1) (middle) and cGP(2) (bottom) method (from T=9 until T=10 after starting from T=0).

DOI: 10.1002/fld

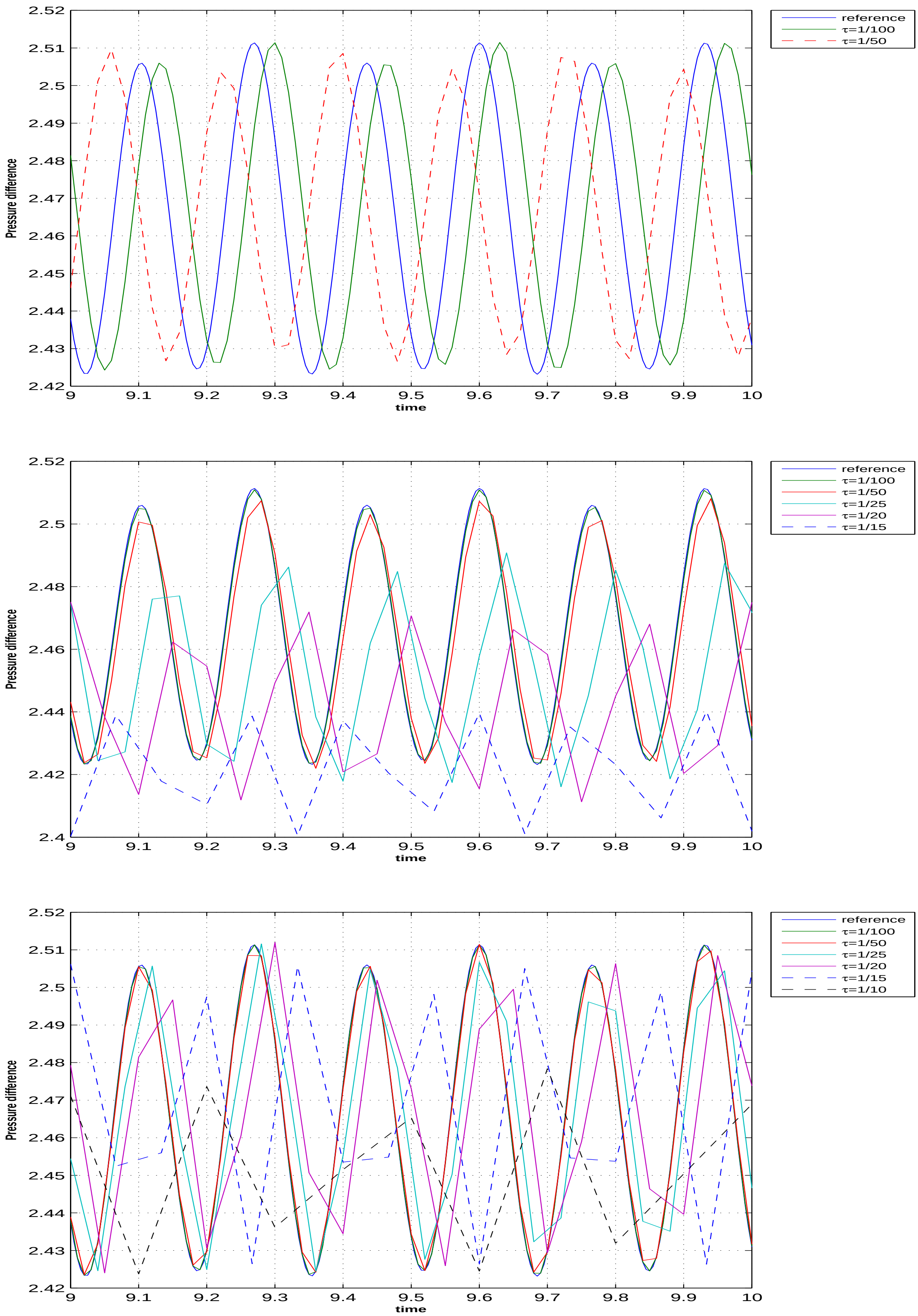

Figure 5. Pressure difference $\Delta p = p_A(0.15, 0.2) - p_B(0.25, 0.2)$ for level 4 for different τ, using cGP(1) (top), dG(1) (middle) and cGP(2) (bottom) method.

Prepared using fldauth.cls
DOI: 10.1002/fld

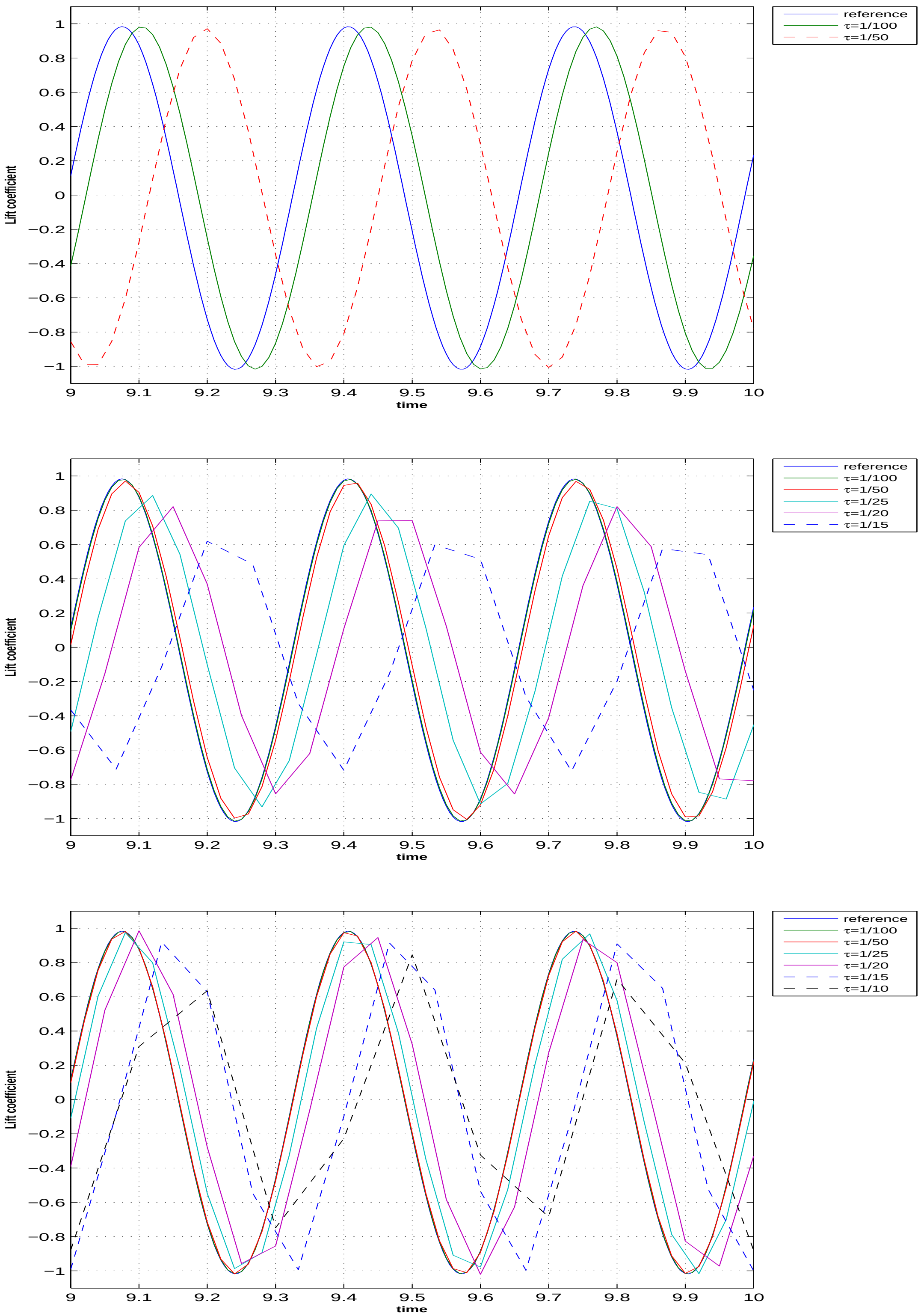

Figure 6. Lift coefficient for level 4 for different τ, using cGP(1) (top), dG(1) (middle) and cGP(2) (bottom) method.

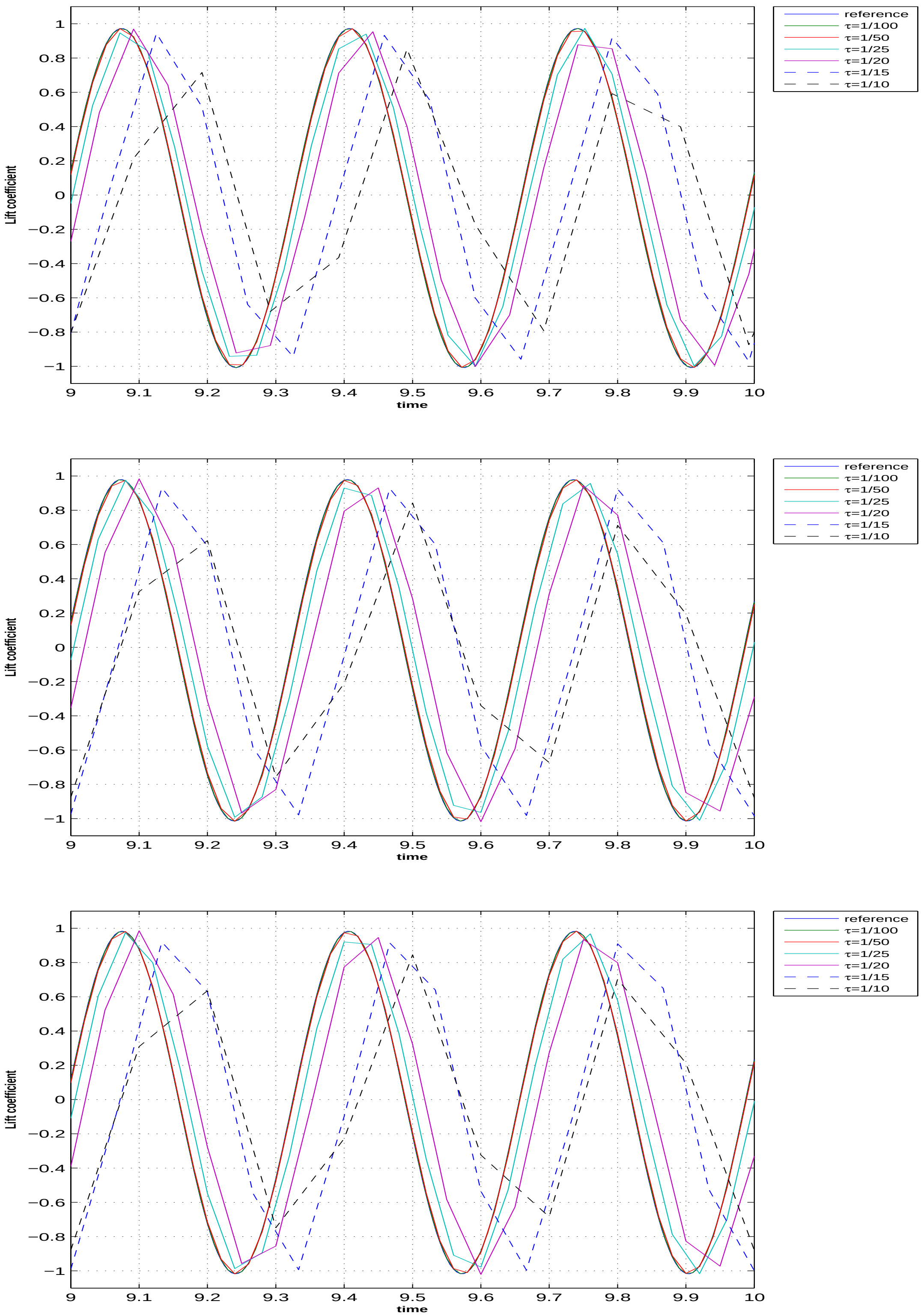

Figure 7. Lift coefficient for different τ, using cGP(2)-method at (space) mesh level 2, 3 and 4.

DOI: 10.1002/fld

Next, we perform a more careful analysis on the basis of the plots already (partially) shown in Figure 4 to 7. To this end, we will mainly concentrate on the values of the lift coefficient (C_L) because this quantity has the larger amplitude in comparison with others. Table I and II demonstrate the 'deviation in percentage of the curves per cycle' for the corresponding time step sizes from the reference values, i.e., $\frac{\Delta x}{30 \times 0.33} \times 100\%$, where Δx is the total deviation after T=10 (with length of period ≈ 0.33, number of cycles until T=10 ≈ 30). The reference values are taken from the higher order cGP(2) scheme with very small time step $\tau = 1/200$ (keep in mind that all tests started from the same start solution and that we perform approximately 30 oscillations until T=10). The different time discretization schemes are then compared in the sense that allows large time steps to gain the desired accuracy.

τ	**cGP(1)**	**cGP(2)**	**dG(1)**
1/100	0.32%	0.00%	0.01%
1/50	1.33%	0.01%	0.05%
1/25		0.12%	0.39%
1/20		0.29%	0.71%
1/15		0.85%	1.61%
1/10		0.98%	

Table I. Deviation of the lift coefficient in percentage for space level=4.

τ	**cGP(1)**	**cGP(2)**	**dG(1)**
1/100	0.32%	0.00%	0.01%
1/50	1.32%	0.01%	0.05%
1/25		0.12%	0.37%
1/20		0.29%	0.68%
1/15		0.85%	1.51%
1/10		0.85%	

Table II. Deviation of the v-velocity at point P(0.4, 0.2) in percentage for space level=4.

In the next Table III, we conclude the maximum allowed time step sizes to gain comparable results with an error of less than 1% per time period at a given space level for the corresponding time discretization schemes.

Lev	**cGP(1)**	**cGP(2)**	**dG(1)**
2	1/100	1/10	1/20
3	1/100	1/10	1/20
4	1/100	1/10	1/20
factor	10	1	2

Table III. Maximum allowed timestep sizes to obtain deviation of less than 1% per time period at given space level for cGP(1) vs. cGP(2) vs. dG(1).

Summarizing the results from Table III, we can see that the corresponding time step sizes to gain the accuracy with an error of less than 1% per time period are two times larger for the cGP(2)- than for the dG(1)-method and ten times larger than for the cGP(1)-method.

DOI: 10.1002/fld

Finally, we want to show all the presented time discretization schemes with those time step sizes for which the lift coefficient (C_L) values are almost identical $(\leq 0.5\%)$ after T=10, resp., approx 30 periods. Figure 8 depicts the corresponding lift coefficients, for 10 time units. We also zoom these quantities in the last time unit (from T=9 until T=10) to see the (very small) differences more clearly in Figure 9.

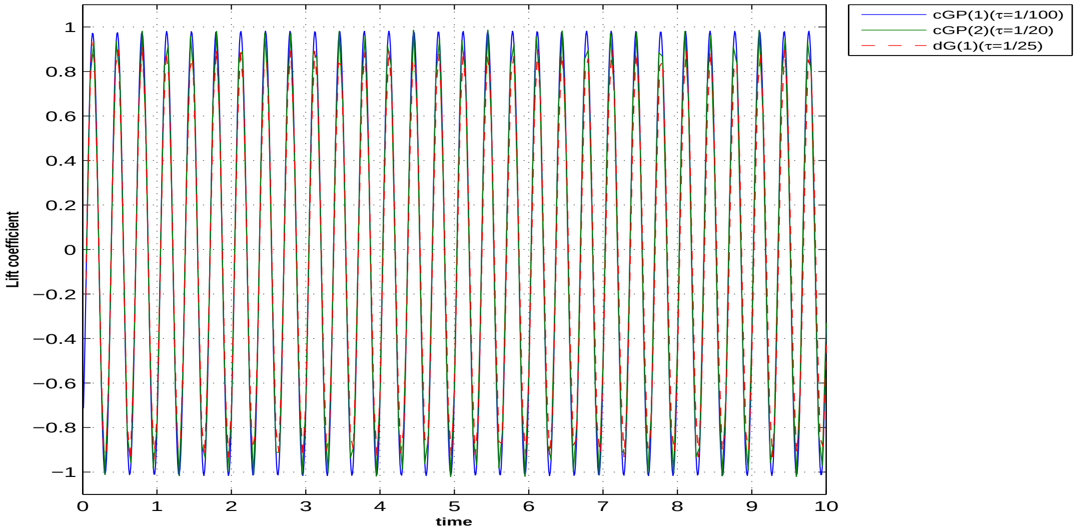

Figure 8. Lift coefficient for cGP(1) vs. cGP(2) vs. dG(1) at space level 4.

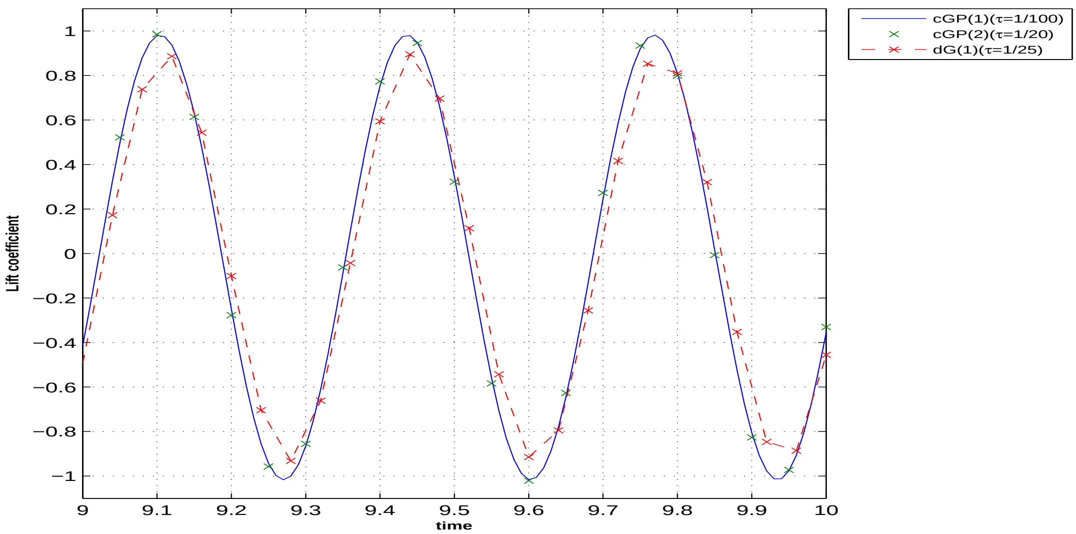

Figure 9. Lift coefficient for cGP(1) vs. cGP(2) vs. dG(1) at space level 4.

DOI: 10.1002/fld

4.2. Nonstationary flow through a Venturi pipe

The test configuration for the 'flow through a Venturi pipe' which is considered here is slightly changed from the framework which has been already used in [5, 6]. Figure 10 shows the geometry and the coarse mesh (level 1) used for this simulation. The coarse mesh is recursively refined by joining opposite midpoints. The total length of the Venturi pipe is $L = 42$, the height of the Venturi pipe at the in/outlet is $H = 5$, the height in the most narrowing part is $H_i = 1$ and the width of the small upper channel is $W_i = 0.8$. The upper, lower walls of the pipe and the sides of the small upper channel are subjected to the no slip boundary conditions. At the inlet (left part of the boundary), an inflow of constant velocity $U = 1$ is prescribed while natural boundary conditions are prescribed at the outlet (right part of the boundary) and at the small upper in/outlet. The value of the kinematic viscosity is set to $\nu = 10^{-2}$ and the density of the fluid $\rho = 1$. The *Reynolds* Re *number* determining the flow properties may be defined as

$$Re = \frac{\overline{U} H_i}{\nu},$$

where $\overline{U}$ is the maximum velocity through the narrow section in the pipe and L is the height of this section. The resulting maximum velocity $\overline{U} \approx 7.0$ yields $Re \approx 700$. The resulting *Reynolds number* produces complex flow patterns which are oscillating in space and time. As we explained before, the aim of the simulation is to control the flux through the upper channel. Beside this interesting flow quantity we also compute the v-velocity at the point $P(16.0, 5.4)$ (top of the small channel) and $P(27.05, 2.5)$ (right of the pipe) and the pressure at the point $P(16.0, 2.5)$ in the middle of the pipe to compare the accuracy of all the presented time discretization schemes. Figure 11 gives an overview of the size of the problem on different space mesh levels where the finite element discretization is carried out by using the biquadratic Q_2-element for the velocity and discontinuous P_1-element for the pressure. Here, we employ the edge oriented jump FEM stabilization approach (see [14]) with stabilization parameter $\gamma = 0.1$. In order to compare the accuracy of different time discretizations,

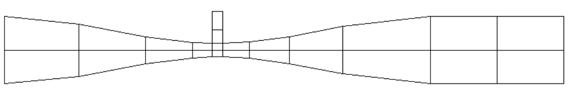

Figure 10. Coarse mesh for the Venturi pipe flow.

Lev.	#EL	#DOF(total)
3	384	4 466
4	1 536	17 378
5	6 144	68 546
6	24 576	272 258

Figure 11. Size of the different systems in space.

the flow is started on each mesh level from the corresponding Stokes solution at time $t = 0$, and the simulation is performed until T=30 using different time discretization methods for different time step sizes τ. At T=30, all the quantities of interest are plotted and analyzed in detail. Since the results obtained from Crank-Nicolson and cGP(1)-method are almost identical as expected, therefore we show the results for cGP(1) only together with the cGP(2) and dG(1)-method.

Prepared using fldauth.cls
DOI: 10.1002/fld

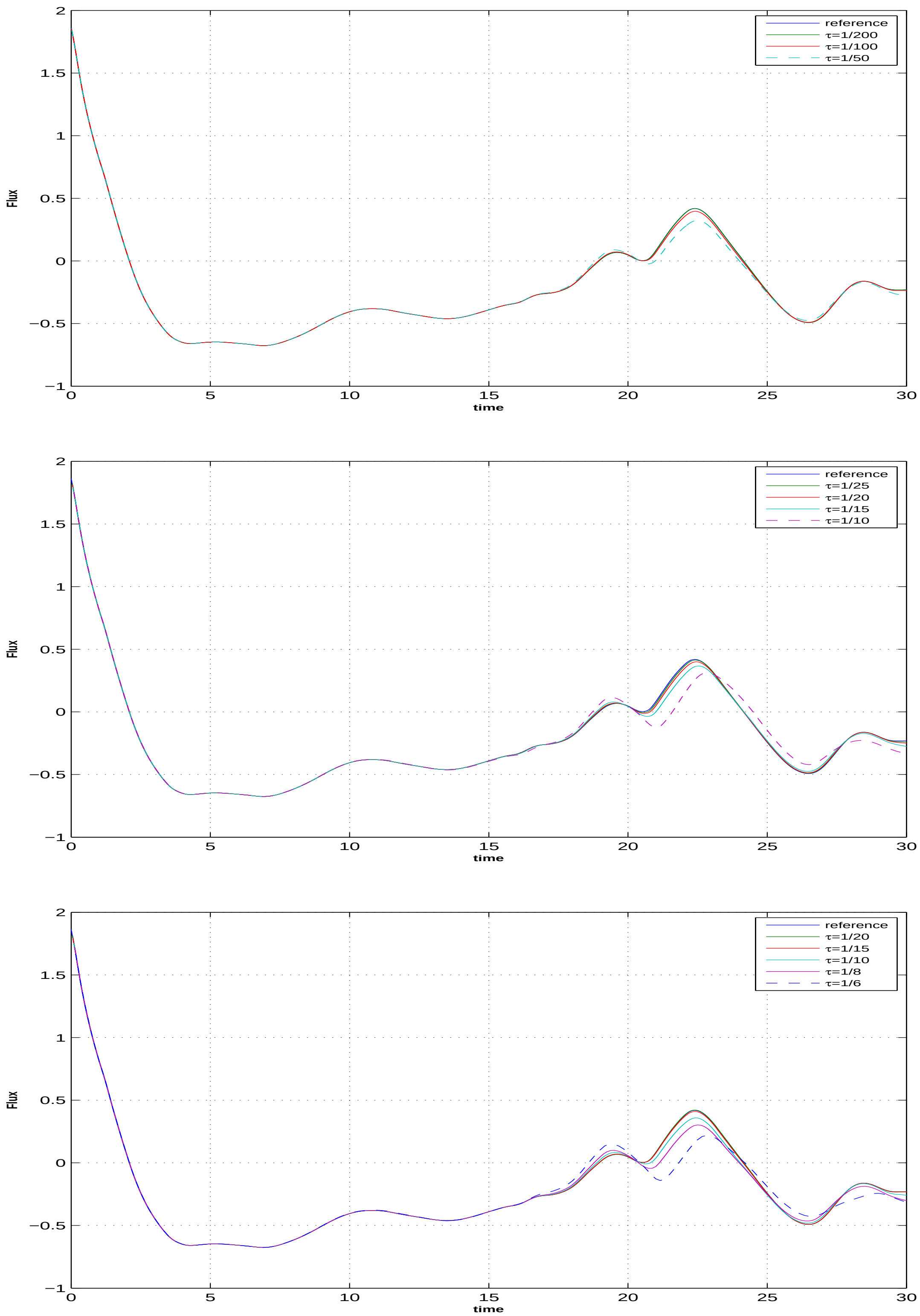

Figure 12. Flux through the upper inlet/outlet at space level 5, using the cGP(1) (top), dG(1) (middle) and cGP(2) (bottom) method.

DOI: 10.1002/fld

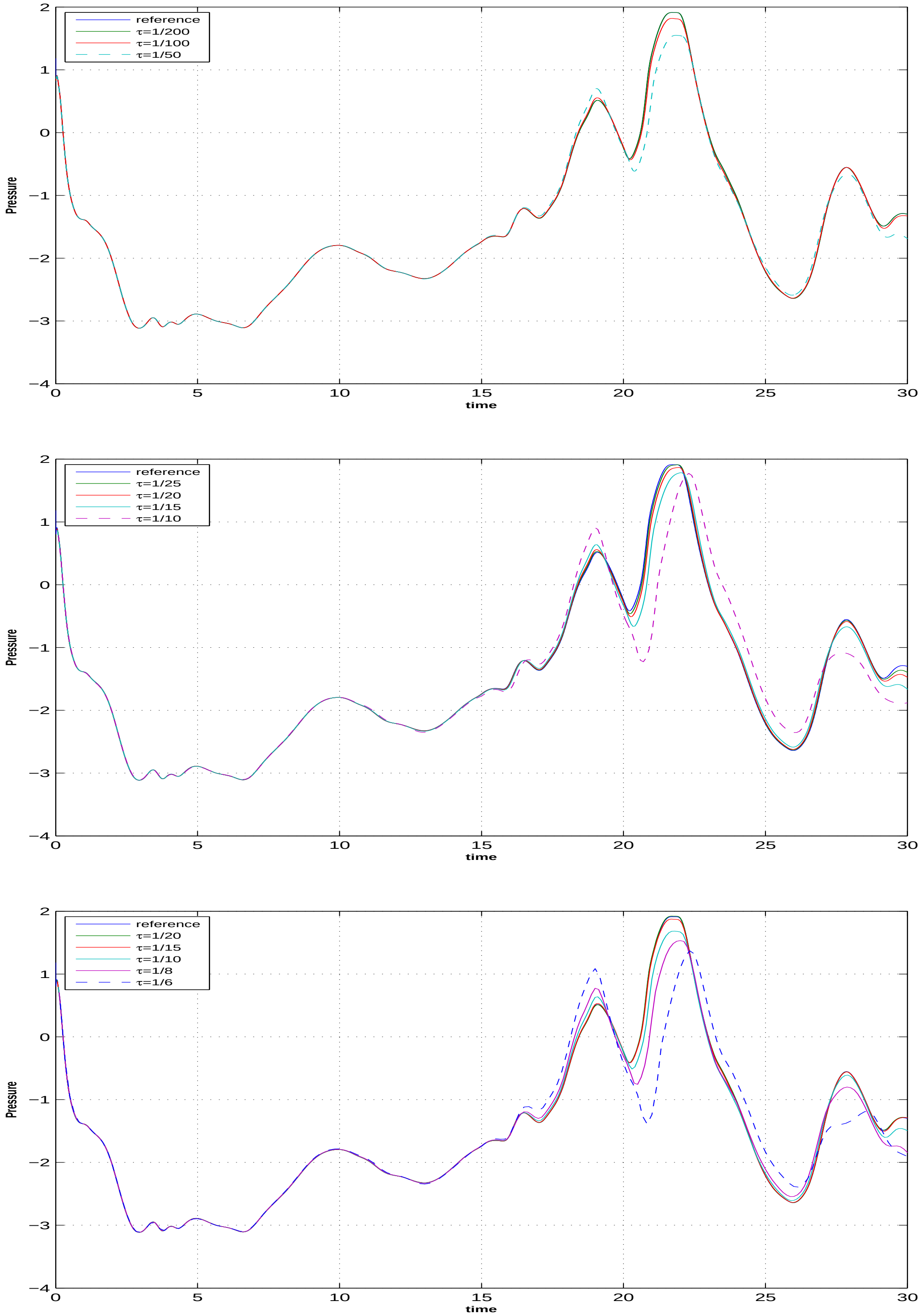

Figure 13. Pressure at point $P(16.0, 2.5)$ at space level 5, using the cGP(1) (top), dG(1) (middle) and cGP(2) (bottom) method.

Prepared using fldauth.cls
DOI: 10.1002/fld

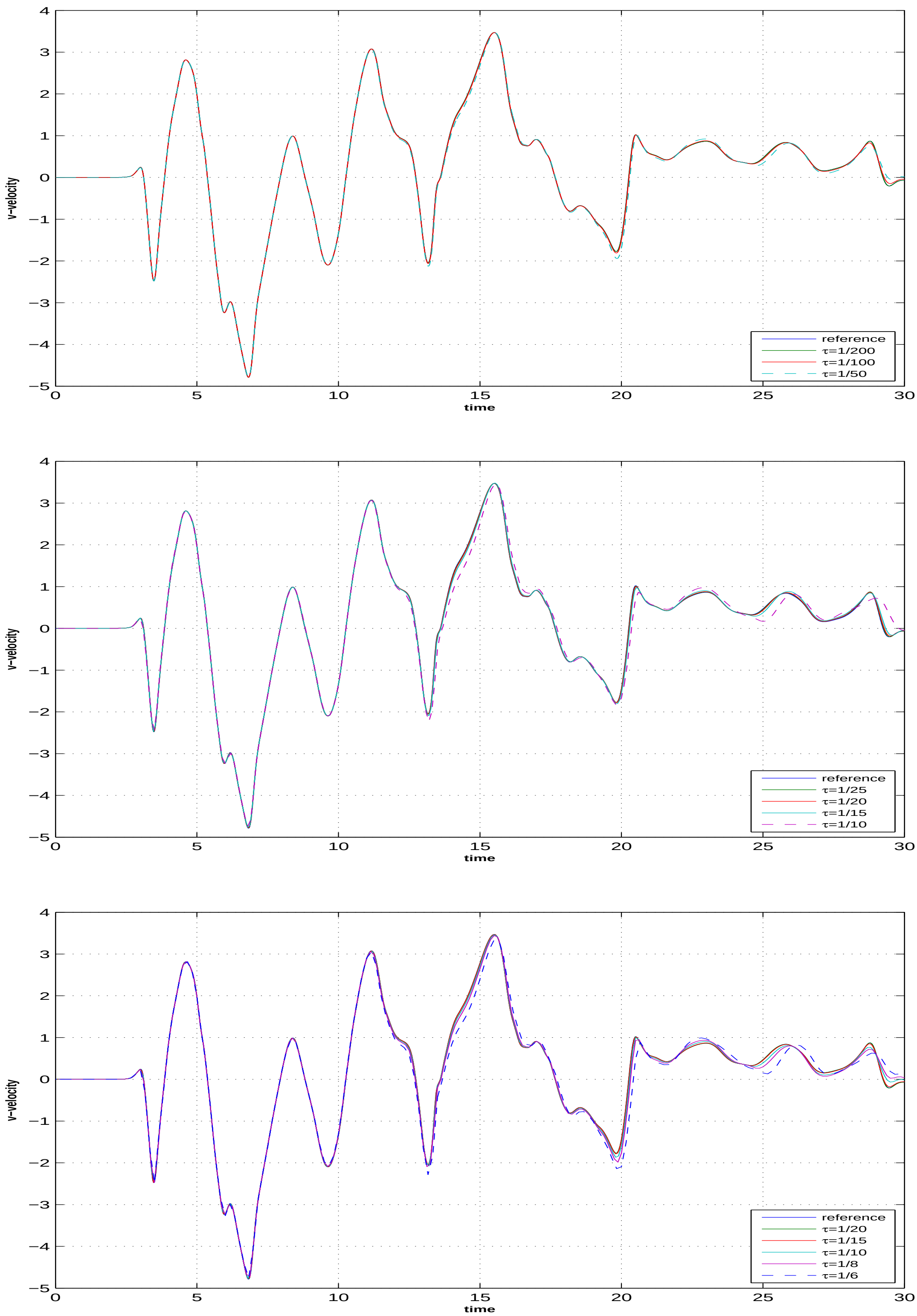

Figure 14. v-velocity at point $P(27.05, 2.5)$ at space level 5, using the cGP(1) (top), dG(1) (middle) and cGP(2) (bottom) method.

We observe from Figure 12 to 14 that the cGP(2)-method captures the dynamics of the flow at quite large time step sizes as expected. The results here on different mesh levels look somewhat more different due to the higher Reynolds number. As in the case of the cylinder before, we demonstrate in the same way the maximum allowed time step sizes which lead to very similar results in the 'picture norm'. Table IV shows these time step sizes for different space mesh levels.

Lev	**cGP(1)**	**cGP(2)**	**dG(1)**
3	1/50	1/5	1/10
4	1/50	1/5	1/10
5	1/100	1/10	1/20
factor	10	1	2

Table IV. Maximum allowed time step sizes which lead (almost) to same results at given space level.

Accordingly, we show the corresponding plots associated to the time steps in Figure 15.

DOI: 10.1002/fld

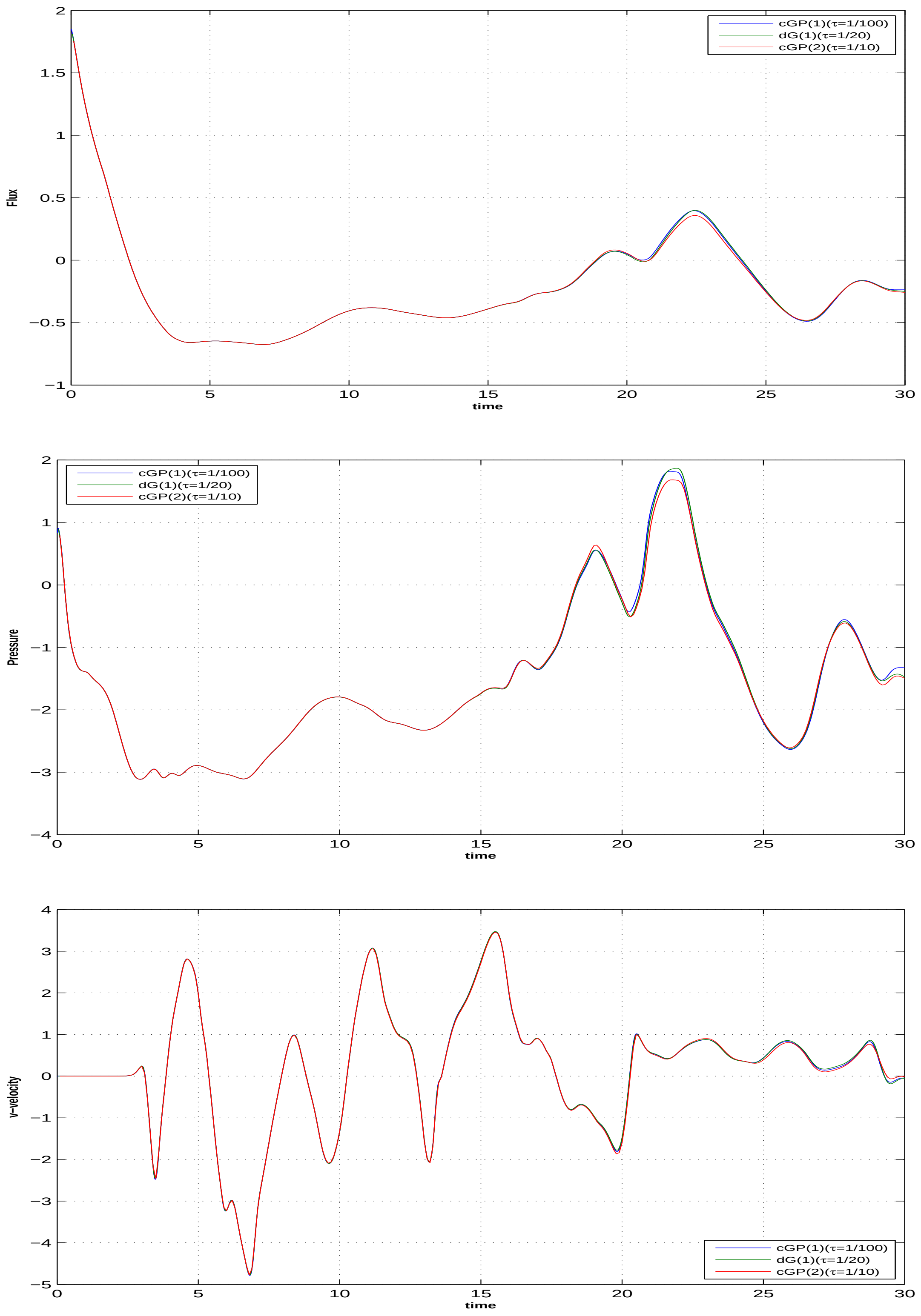

Figure 15. Flux (top)/pressure (middle)/v-velocity (bottom) at point $P(27.05, 2.5)$ at space level 5, using the cGP(1) vs. dG(1) vs. cGP(2)-method with max. allowed time steps.

Finally, we demonstrate how the solution patterns develop in the last 13 time units from T=18 to T=30. Figure 16 illustrates the velocity at space level 5.

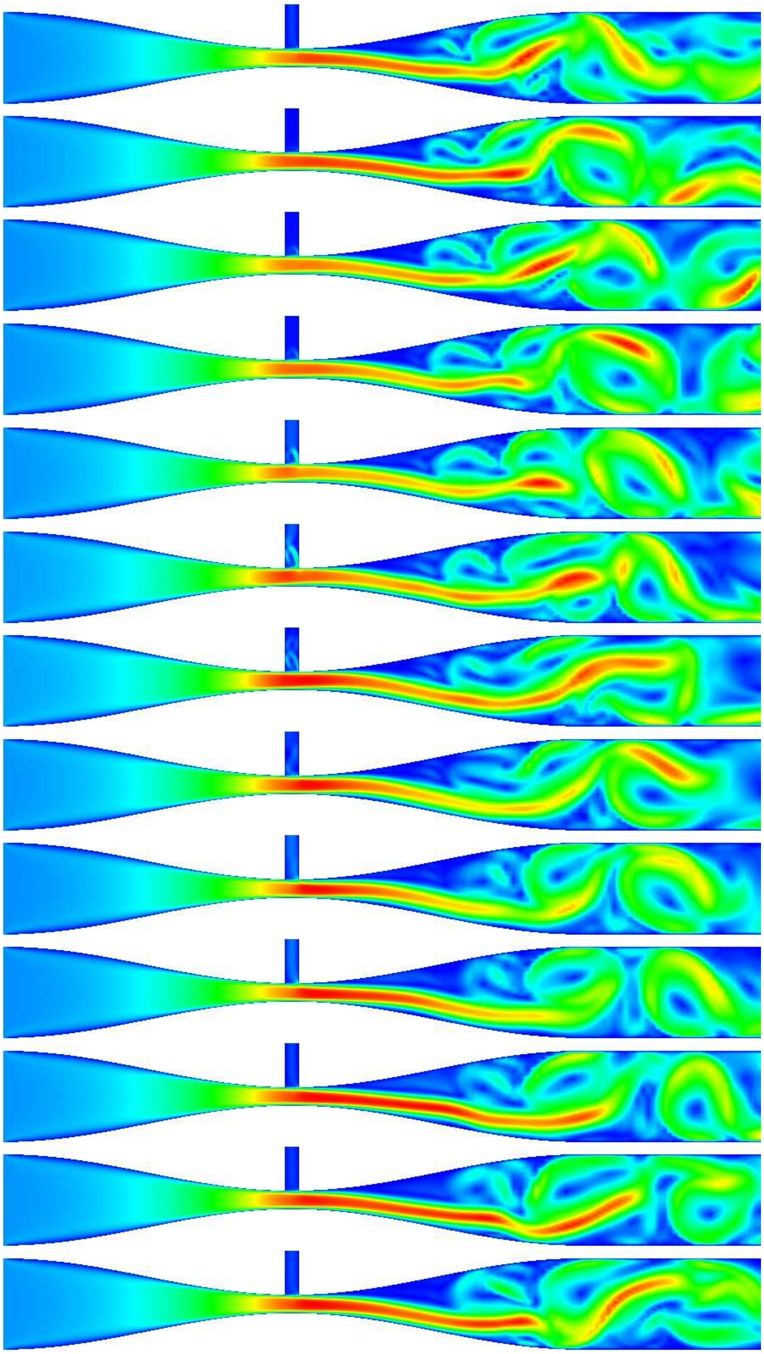

Figure 16. Visualization of the velocity magnitude in the Venturi pipe at space level 5 for 13 subsequent time units.

DOI: 10.1002/fld

5. CONCLUSION

We have described in detail the application of the class of *continuous* Galerkin-Petrov and *discontinuous* Galerkin time discretization schemes to the nonstationary incompressible Navier-Stokes equations. The first higher order members of these classes, namely the cGP(2)- and the dG(1)-method, are superconvergent of 4th and 3rd order at the endpoints of the time intervals, respectively. The spatial FEM discretization has been carried out by using conforming biquadratic elements for velocity and discontinuous linear elements for pressure on a quadrilateral mesh leading to 3rd order accuracy in space for the L^2-norm of the velocity. The discretized systems of nonlinear equations are linearized by means of the Newton method, and the associated linear systems have been solved using a geometrical multigrid method with a Vanka-type preconditioned GMRES method as smoother.

For the evaluation of our approach, we performed numerical simulations for two nonstationary benchmarking flow configurations in order to compare the performance of the various temporal discretizations. For these two test problems, the classical *flow around cylinder* configuration and the nonstationary *flow through a Venturi pipe*, we can summarize as a result that the cGP(2)-method allows approximately for a 10 times larger time step size than the cGP(1)-method (or Crank-Nicolson scheme) to achieve the same accuracy, while the dG(1)-method allows approximately for a factor of 5. Since the corresponding analysis (see [15]) of the numerical costs for the cGP(2)- and dG(1)-method shows that the arising nonlinear block-systems in the implicit time discretization schemes can be solved very efficiently with nearly optimal complexity, this higher order approach is clearly advantageous in comparison to classical second order time stepping schemes.

REFERENCES

1. Hussain S, Schieweck F, Turek S. Higher order Galerkin time discretizations and fast multigrid solvers for the heat equation. *Journal of Numerical Mathematics* 2011; **19**(1):41–61.
2. Hussain S, Schieweck F, Turek S. A note on accurate and efficient higher order Galerkin time stepping schemes for the nonstationary Stokes equations. *The Open Numerical Methods Journal* 2012; **4**:35–45.
3. Damanik H, Hron J, Ouazzi A, Turek S. Monolithic Newton–multigrid solution techniques for incompressible nonlinear flow models. *International Journal for Numerical Methods in Fluids* 2012; Accepted.
4. Turek S, Schäfer M. Benchmark computations of laminar flow around cylinder. *Flow Simulation with High-Performance Computers II*, *Notes on Numerical Fluid Mechanics*, vol. 52, Hirschel E (ed.), Vieweg, 1996; 547–566.
5. Turek S. *Efficient solvers for incompressible flow problems. An algorithmic and computational approach*, *Lecture Notes in Computational Science and Engineering*, vol. 6. Springer, 1999.
6. Turek S. A comparative study of some time-stepping techniques for the incompressible navier-stokes equations: from fully implicit nonlinear schemes to semi-implicit projection methods. *Int. J. Numer. Meth. Fluids* 1996; **22**:987 – 1011.
7. Aziz AK, Monk P. Continuous finite elements in space and time for the heat equation. *Math. Comp.* 1989; **52**(186):255–274.
8. Heywood J, Rannacher R, Turek S. Artificial boundaries and flux and pressure conditions for the incompressible Navier–Stokes equations. *International Journal for Numerical Methods in Fluids* 1996; **22**:325–352.
9. Schieweck F. A-stable discontinuous Galerkin-Petrov time discretization of higher order. *J. Numer. Math.* 2010; **18**(1):25 – 57.
10. Thomée V. *Galerkin finite element methods for parabolic problems*, *Springer Series in Computational Mathematics*, vol. 25. Second edn., Springer-Verlag: Berlin, 2006.

Prepared using fldauth.cls
DOI: 10.1002/fld

11. C Cuvelier, A Segal, A A Steenhoven. *Finite element methods and Navier-Stokes equations*. D. Reidel Publishing Company, 1986.
12. Johnson C. *Numerical Solution of Partial Differential Equations by the Finite Element Method*. Cambridge University Press New York, 1988.
13. Donea J, Huerta A. *Finite element methods for flow problems*. JohnWiley and Sons, New York, 2003.
14. Turek S, Ouazzi A. Unified edge–oriented stabilization of nonconforming FEM for incompressible flow problems: Numerical investigations. *Journal of Numerical Mathematics* 2007; **15**(4):299–322.
15. Hussain S, Schieweck F, Turek S. Fast and efficient solution techniques for coupled block-systems arising from higher order discretization in space and time of the incompressible Navier-Stokes equations 2012. To appear.
16. Wobker H, Turek S. Numerical studies of Vanka-type smoothers in Computational Solid Mechanics. *Advances in Applied Mathematics and Mechanics* 2009; **1**(1):29–55.
17. Hackbusch W. *Multi-Grid Methods and Applications.* Springer-Verlag, Berlin, 1985.

DOI: 10.1002/fld